



Article

Diagnostics of Es Layer Scintillation Observations Using FS3/COSMIC Data: Dependence on Sampling Spatial Scale

Lung-Chih Tsai ^{1,2,*}, Shin-Yi Su ², Chao-Han Liu ³, Harald Schuh ^{4,5} , Jens Wickert ^{4,5}
and Mohamad Mahdi Alizadeh ^{4,6}

- ¹ GPS Science and Application Research Center, National Central University (NCU), Taoyuan 320317, Taiwan
² Center for Space and Remote Sensing Research, National Central University (NCU), Taoyuan 320317, Taiwan; sysu@csrsr.ncu.edu.tw
³ Academia Sinica, Taipei 115024, Taiwan; chliu2@gate.sinica.edu.tw
⁴ Institute of Geodesy and Geoinformation Science, Technische Universität Berlin, 10623 Berlin, Germany; schuh@gfz-potsdam.de (H.S.); wickert@gfz-potsdam.de (J.W.); alizadeh@tu-berlin.de (M.M.A.)
⁵ German Research Centre for Geosciences GFZ, 14473 Potsdam, Germany
⁶ Department of Geodesy and Geomatics Engineering, K. N. Toosi University of Technology, Tehran 19697, Iran
* Correspondence: lctsay@csrsr.ncu.edu.tw

Abstract: The basic theory and experimental results of amplitude scintillation from GPS/GNSS radio occultation (RO) observations on sporadic E (Es) layers are reported in this study. Considering an Es layer to be not a “thin” irregularity slab on limb viewing, we characterized the corresponding electron density fluctuations as a power-law function and applied the Rytov approximation to simulate spatial spectrum of amplitude fluctuations. The scintillation index S_4 and normalized signal amplitude standard deviation S_2 are calculated depending on the sampling spatial scale. The theoretical results show that both S_4 and S_2 values become saturated when the sampling spatial scale is less than the first Fresnel zone (FFZ), and S_4 and S_2 values could be underestimated and approximately proportional to the logarithm of sampled spatial wave numbers up to the FFZ wave number. This was verified by experimental analyses using the 50 Hz and de-sampled FormoSat-3/Constellation Observing System for Meteorology, Ionosphere and Climate (FS3/COSMIC) GPS RO data in the cases of weak, moderate, and strong scintillations. The results show that the measured S_2 and S_4 values have a very high correlation coefficient of >0.97 and a ratio of ~ 0.5 under both complete and undersampling conditions, and complete S_4 and S_2 values can be derived by dividing the measured undersampling S_4 and S_2 values by a factor of 0.8 when using 1-Hz RO data.

Keywords: ionospheric scintillation; ionospheric Es layer; GPS/GNSS radio occultation observation; COSMIC



Citation: Tsai, L.-C.; Su, S.-Y.; Liu, C.-H.; Schuh, H.; Wickert, J.; Alizadeh, M.M. Diagnostics of Es Layer Scintillation Observations Using FS3/COSMIC Data: Dependence on Sampling Spatial Scale. *Remote Sens.* **2021**, *13*, 3732. <https://doi.org/10.3390/rs13183732>

Academic Editor: Guillermo Gonzalez-Casado

Received: 24 August 2021

Accepted: 14 September 2021

Published: 17 September 2021

Publisher’s Note: MDPI stays neutral with regard to jurisdictional claims in published maps and institutional affiliations.



Copyright: © 2021 by the authors. Licensee MDPI, Basel, Switzerland. This article is an open access article distributed under the terms and conditions of the Creative Commons Attribution (CC BY) license (<https://creativecommons.org/licenses/by/4.0/>).

1. Introduction

Sporadic E (Es) layers exhibit ionization enhancements in the E region at altitudes usually between 90 and 120 km [1]. A characteristic feature of Es layers is that they are thin layers of a few kilometers’ thicknesses and a 10–1000 km horizontal extension. Over the past few decades, since the 1950s, Es layers have been extensively studied using a variety of instruments, including ionosondes, incoherent scatter radars and coherent scatter very high-frequency (VHF) radars operating from the ground and in rocket payloads with in-situ measurements. Several excellent reviews of the theories and observations of ionospheric Es layers have also been published [1–4]. It is generally believed that Es layer structure is affected by the plasma convergence effect of neutral wind shear through ion-neutral collision processes at mid and low latitudes [1]. Es layers could appear as non-uniform wave layers, a composition of irregular elongated clouds of intense ionization, or multiple layers, occurring simultaneously and separated by several kilometers within the lower E region [5]. Therefore, this gradient plasma instability can give rise to irregularities, with

scale-sizes from a few tens of meters to a few kilometers, which can produce VHF/UHF radio wave scattering, and cause signal scintillations in satellite radio communication and navigation system performance [6].

The Global Positioning System (GPS) or Global Navigation Satellite System (GNSS) RO techniques provide an innovative view of the ionosphere via horizontal limb sounding from GPS/GNSS satellites to low-Earth-orbiting (LEO) satellites. There have been many successful GNSS-LEO RO missions, such as GPS/Meteorology, the Danish Ørsted, the German CHAMP (Challenging Mini-satellite Payload), the U.S.–German GRACE (Gravity Recovery and Climate Experiment), the GPS-IOX (Ionospheric Occultation Experiment), the Argentinean SAC-C (Satellite de Aplicaciones Cientificas-C), the Taiwan–U.S. COSMIC, and the Taiwan–U.S. COSMIC2. Based on these GPS/GNSS RO missions' data, more Es layer studies have been presented [5,7–11]. Notably, in most of the above investigations, the criteria to identify Es events include that the peak normalized amplitude standard deviation of GPS/GNSS RO observations at E-region altitudes is higher than 0.2. However, this presents a problem for scintillation data for which the limb-viewing amplitudes of some of the GNSS-LEO RO missions were obtained at a sampling frequency less than the Fresnel frequency f_F , i.e., a sampling spatial scale larger than the first Fresnel zone (FFZ). Such undersampling had not happened in earlier Es layer investigations using incoherent scatter radars and coherent scatter VHF radars operating from the ground and in rocket payloads with in situ measurements. Thus, it is desirable to clarify the dependence on sampling spatial scale of scintillation index determination, and find a method of solving reliable scintillation indexes (S_4 and S_2) under undersampling conditions on GPS/GNSS RO observations.

In the following section, we introduce the Ryton approximation for radio wave propagations through an Es layer irregularity slab, and simulate the scintillation index S_4 and normalized signal amplitude standard deviation S_2 values, depending on the sampling spatial scale. In Section 3, we analyze the 50 Hz FS3/COSMIC RO amplitude data and the corresponding de-sampled data to prove the dependence of S_4 and S_2 determinations on sampling spatial scale. In Section 4, we present the reliability of complete S_4 and S_2 determinations using undersampling S_4 and S_2 measurements. In conclusion, we summarize the usefulness of the results.

2. Methods and Materials

When a radio wave transmitted by a satellite passes through the ionosphere, its wavefront will be distorted by irregular electron densities, i.e., plasma densities. After the radio wave has emerged from an irregularity slab, its phase front is randomly modulated. It is assumed that the deviation and the change in the refractive index over a spatial range of one wavelength and a temporal range of one wave period are slight. Under such a condition, the small-angle scattering of a layer of plasma density turbulence causes spatial and temporal fluctuations of radio wave intensity and phase, which is known as scintillation. In this study, we focus on the diagnostics of amplitude scintillation during GPS/GNSS RO observations carried out on Es layers.

Let us assume the geometry of an Es layer scintillation problem in GPS/GNSS RO observations, as shown in Figure 1. A region of irregular electron density structures is located from $x = -L/2$ to $x = L/2$, where L could be the cutoff length of a GPS-LEO limb viewing link through an Es layer. A time-harmonic electromagnetic wave is transmitted by a GNSS satellite located at $x = -\infty$, and it is incident on an Es layer slab at $x = -L/2$ and received by an LEO satellite receiver at a specific coordinate (x, ρ_t) , where $\rho_t = (y, z)$ is the transverse coordinate of wave propagation. The small-angle scattering of the scintillation phenomenon reduces the propagation equation of a wave field, where $E = u(x, \rho_t) \exp(-ikx)$, to the parabolic wave equation in $u(x, \rho_t)$, as follows [12].

$$-2jk \frac{\partial u}{\partial x} + \nabla_t^2 u = -k^2 \varepsilon_1(x, \rho_t) u, \quad (1)$$

where $-L/2 < x < L/2$, and $\nabla_t^2 = \partial^2/\partial_y^2 + \partial^2/\partial_z^2$.

$$-2jk \frac{\partial u}{\partial x} + \nabla_t^2 u = 0, \quad (2)$$

where $x > L/2$. Here, $\varepsilon_1(x, \rho_t)$ is the fluctuating part of dielectric permittivity $\varepsilon(x, \rho_t)$. Equations (1) and (2) are of the parabolic type, whose solutions are determined uniquely by the boundary conditions at $x = -L/2$ and $x = L/2$, respectively. Notably, the irregularity slab can be characterized by its dielectric permittivity, as follows.

$$\varepsilon(x, \rho_t) = \langle \varepsilon \rangle [1 + \varepsilon_1(x, \rho_t)] = [1 - (f_{p0}/f)^2] \varepsilon_0 [1 + \varepsilon_1(x, \rho_t)], \quad (3)$$

and

$$\varepsilon_1(x, \rho_t) = -\frac{(f_{p0}/f)^2 [\Delta N(x, \rho_t)/N_0]}{1 - (f_{p0}/f)^2} \approx -\frac{e^2}{4\pi^2 \varepsilon_0 m f^2} \Delta N(x, \rho_t), \quad (4)$$

where $\Delta N(x, \rho_t)$ is the fluctuating part of electron density, and f_{p0} is the plasma frequency corresponding to the background electron density N_0 . f is the radio wave frequency, i.e., GPS L1- or L2-band frequency, and is much larger than f_{p0} . The other constants include the electronic charge e , the electronic mass m , and the free space permittivity ε_0 . Notably, $\varepsilon_1(x, \rho_t)$ is proportional to the fluctuating part of electron density $\Delta N(x, \rho_t)$ but is in inverse proportion to the square of radio wave frequency f . In this study, we do not consider the effects of wave propagation through an elongated Es layer cloud and/or multiple Es layers. It will be interesting to work on this in future investigations.

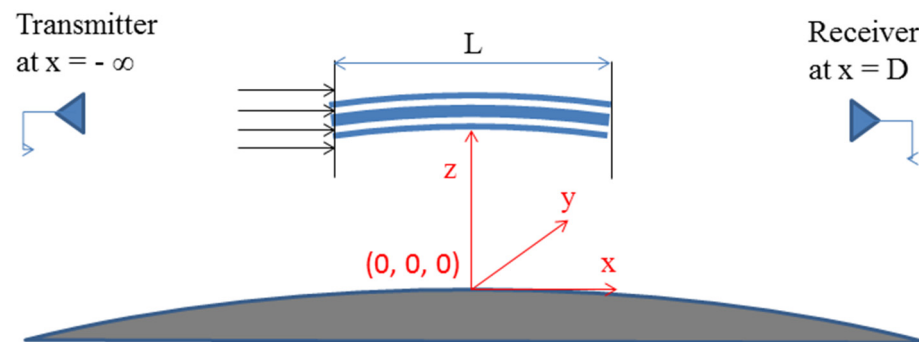


Figure 1. Geometry of an Es layer scintillation problem on GPS/GNSS RO observations. The origin is allocated as the point at which the Es layer's center is projected onto the Earth's surface. The x and z axes point in the GPS-LEO limb's viewing direction and the azimuth direction, respectively.

It is now generally accepted that ionospheric electron density irregularities can be characterized by a power-law function [3,13–16]. To characterize the general power-law irregularity spectrum with spatial index p , [17] introduced a fairly general correlation spectrum, as follows.

$$\Phi_{\Delta N}(\kappa) = \frac{\sigma_N^2 \Gamma(\frac{p}{2}) \kappa_0^{p-3}}{\pi^{3/2} \Gamma(\frac{p-3}{2})} (\kappa^2 + \kappa_0^2)^{-p/2} \propto \kappa^{-p}, \quad (5)$$

where κ_0 is the wave number of the outer scale $l_0 (=2\pi/\kappa_0)$ in an irregularity slab, and $\Gamma(\cdot)$ is the Gamma function. The outer scale is defined as an intrinsic property of the instability that causes electron density and plasma irregularities. The power-law continuum encompasses at least three orders of magnitude in the spatial scale size [13]. Notably, the power-law spectrum is expected to be valid when its spatial scale is much less than the outer scale. In practice, it conforms to a GPS-LEO limb viewing an Es layer with a 10~1000 km horizontal extension.

Historically, the first ionospheric scintillation theory was based on the idea of wave diffraction from a phase-changing screen, and named phase screen theory [14,15,18]. This assumes that, as the radio waves propagate through an irregularity slab, to the first order, only the phase is affected by the random fluctuations in refractive index. The phase screen theory can be applied for the weak scintillations usually induced by a “thin” irregularity slab. Ref. [11] derived an Es layer thickness of 1.2 km at a peak distribution based on the 50 Hz “atmPhs” FS3/COSMIC data. Considering such an Es layer distributed at an altitude of 100 km and along the Earth’s curvature, the cutoff length of a GPS-LEO limb’s viewing link through the Es layer is approximately 160 km, taken as the value of L in Figure 1. Therefore, we consider here that the Es layer in limb viewing is not a thin irregularity slab. The effects of scattering on the field amplitude inside a limb viewing irregularity slab must be included in the treatment of the Es layer scintillation phenomenon. Earlier investigations [13,19,20] derived the Ryton approximation for the parabolic wave Equations (1) and (2), and concluded that the Ryton approximation can be applied to weak and even strong ionospheric scintillations. Using the Ryton approximation, a wave field can be presented in terms of the fluctuation of a complex phase $\psi(x, \rho_t)$, shown as follows:

$$u(x, \rho_t) = u_0 \exp[\psi(x, \rho_t)] = u_0 \exp[\chi(x, \rho_t) - jS_1(x, \rho_t)], \quad (6)$$

where u_0 is the average field of $u(x, \rho_t)$ and is a reference field with definite amplitude and phase. $\chi(x, \rho_t)$ and $S_1(x, \rho_t)$ are referred to as the log-amplitude and the phase departure of a wave field, respectively. The general Ryton solution of the parabolic wave Equations (1) and (2) was obtained as follows.

$$\psi(x, \rho_t) = \frac{jk}{2\pi(x+L/2)} \iint \psi_0(-L/2, \rho'_t) \exp\left[\frac{-jk|\rho_t - \rho'_t|^2}{2(x+L/2)}\right] d^2\rho'_t + \frac{k^2}{4\pi} \int_{-\frac{x}{2}}^x \frac{d\zeta}{x-\zeta} \iint \varepsilon_1(\zeta, \rho'_t) \exp\left[\frac{-jk|\rho_t - \rho'_t|^2}{2(x-\zeta)}\right] d^2\rho'_t, \quad (7)$$

where $-L/2 < x < L/2$.

$$\psi(x, \rho_t) = \frac{jk}{2\pi(x-L/2)} \iint \psi(L/2, \rho'_t) \exp\left[\frac{-jk|\rho_t - \rho'_t|^2}{2(x-L/2)}\right] d^2\rho'_t, \quad (8)$$

where $x > L/2$. Notably, $\psi_0(-L/2, \rho_t) = \ln u(-L/2, \rho_t)$ corresponds to the incident wave of the irregular slab, and $\psi(L/2, \rho_t) = \ln u(L/2, \rho_t)$ is its boundary condition at $x = L/2$.

In this study, we develop a plane incident wave with unity amplitude to be incident on an Es layer slab in a limb-viewing direction. The small scattering angle assumption means that the mean values of the log-amplitude and phase departures of the wave field through an Es layer slab are approximately zero, i.e., $\langle \chi \rangle \sim \langle S_1 \rangle \sim 0$. The power spectra for χ and S_1 are given, respectively, by [21], as follows.

$$\Phi_\chi(0, \kappa_t) = \frac{\pi k^2 L}{4} \left[1 - \frac{2k}{\kappa_t^2 L} \sin\left(\frac{\kappa_t^2 L}{2k}\right) \cos\left(\frac{\kappa_t^2 (x-L/2)}{k}\right) \right] \Phi_{\varepsilon_1}(0, \kappa_t). \quad (9)$$

$$\Phi_{S_1}(0, \kappa_t) = \frac{\pi k^2 L}{4} \left[1 + \frac{2k}{\kappa_t^2 L} \sin\left(\frac{\kappa_t^2 L}{2k}\right) \cos\left(\frac{\kappa_t^2 (x-L/2)}{k}\right) \right] \Phi_{\varepsilon_1}(0, \kappa_t). \quad (10)$$

As shown in Figure 1, x is the distance from the center of an irregularity slab to the receiver on an LEO satellite, and is equal to D (~ 3500 km) for a GPS/GNSS RO observation on Es layers. κ_t is the wave number of a transverse spatial scale ρ_t . Notably, the spatial power spectrum of the log amplitude departure of wave field is controlled by two competing factors: a Fresnel filter function, shown as the expression in the square brackets in Equation (9), and the power-law function of dielectric permittivity or electron density fluctuation. Figure 2 shows the Fresnel filter as a function of normalized wave number κ_t/κ_F , where $\kappa_F (=2\pi/D_F)$ is the wave number in the first Fresnel zone (FFZ) $D_F (= \sqrt{\lambda D} \sim 0.8$ km)

corresponding to the GPS L1-band signal and a distance D of approximately 3500 km from the Es layer slab to the LEO satellite during a GPS/GNSS RO observation. The oscillatory character of the filter function is known as the Fresnel oscillation [3]. In Figure 2, the spatial power spectrum of the simulated log amplitude departure of wave field from Equation (9) is also shown at a spatial index p of 4. The spatial spectrum is generally of a power-law type with an order of p that decays as κ_t increases. It has a maximum around $\kappa_t = \kappa_F$, corresponding to the first maximum of the Fresnel filter function. This is consistent with an irregularity size in the order of FFZ, which is most effective in causing amplitude scintillation.

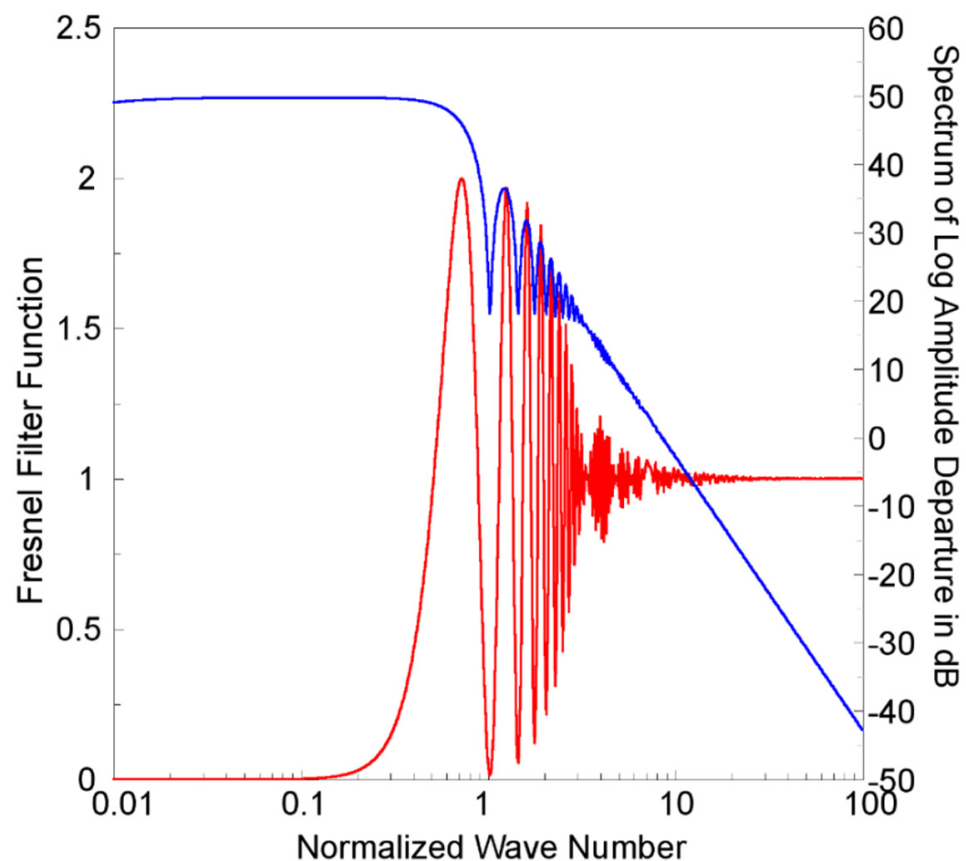


Figure 2. A Fresnel filter function of normalized wave number κ_t/κ_F in log scale (shown as the red line). The theoretical spectrum of the log amplitude departure of the wave field as a function of the normalized wave number κ_t/κ_F is also shown as the blue line.

Applying the Wiener–Khinchin theorem [12] and Equations (3)–(5) and (9), the correlation of the log amplitude departure of the wave field can be derived by its spatial power spectrum, as follows.

$$\begin{aligned} \langle \chi^2 \rangle &= B_\chi(0) = \iint \Phi_\chi(0, \kappa_t) d^2\kappa_t \\ &= \frac{\sigma_N^2 \Gamma(\frac{p}{2}) L}{2^{\frac{p}{2}} \pi^{\frac{p+1}{2}} \Gamma(\frac{p-3}{2})} \iint \left[1 - \frac{1}{\pi} \frac{\kappa_f^2}{\kappa_t^2} \frac{x}{L} \sin\left(\pi \frac{\kappa_t^2}{\kappa_f^2} \frac{L}{x}\right) \cos\left(2\pi \frac{\kappa_f^2}{\kappa_t^2} \frac{(x-\frac{L}{2})}{x}\right) \right] \frac{\kappa_0^{p-3} k^2 - p/2 x^{p/2}}{\left(\frac{\kappa_t^2}{\kappa_f^2} + \frac{\kappa_0^2}{\kappa_f^2}\right)^{p/2}} d^2\kappa_t, \end{aligned} \tag{11}$$

As a measure of amplitude scintillation, the scintillation index S_4 is most often used and is defined as a normalized variance of signal power intensity I , as follows.

$$S_4^2 = \frac{\langle (I - \langle I \rangle)^2 \rangle}{\langle I \rangle^2}. \tag{12}$$

Applying Ryton approximation, it is natural to suppose that the logarithmic amplitude has a normal distribution with a mean of zero because of the small angle scattering through an irregularity slab. Therefore, $\langle \chi \rangle$ and $\langle \chi^3 \rangle$ are approximately zero, and can be neglected, and $\langle \chi^4 \rangle = 3\langle \chi^2 \rangle^2$. Considering the moderate or strong scintillations as radio waves propagate through an Es layer's irregularity slab, we include the first four orders of the Taylor series in our exponential functions and obtain

$$S_4^2 = \frac{\langle u_0^4 \exp(4\chi) \rangle}{\langle u_0^2 \exp(2\chi) \rangle^2} - 1 \approx \frac{4\langle \chi^2 \rangle + 24\langle \chi^2 \rangle^2}{1 + 4\langle \chi^2 \rangle + 8\langle \chi^2 \rangle^2}. \quad (13)$$

Notably, the square of the S_4 value is a function of the log amplitude departure correlation of wave field, i.e., $\langle \chi^2 \rangle$. Equation (13) indicates that, for weak scintillations, i.e., $\langle \chi^2 \rangle \ll 1$, $S_4^2 \sim 4\langle \chi^2 \rangle$, and the S_4 value is approximately equal to double the square root of the integral of the log amplitude departure spectra in the spatial scale.

In practical situations of GPS/GNSS RO observations, the radio signals are transmitted from a GPS/GNSS satellite and received by an LEO satellite at an altitude of approximately 100 km. The projected speed v_z of the LEO satellite in the azimuth direction, i.e., the z direction in Figure 1, is approximately 3.2 km/s, which is much faster than the projected speed of the GPS/GNSS satellite and also the drift speed of the Es layer irregularities along the z direction. The temporal variations in GPS/GNSS signals received by an LEO receiver can be considered as the result of radio beam scanning over the z -direction variations of frozen Es layer irregularities. Therefore, the sampling frequency f_s on GPS/GNSS RO observations can be transferred to the wave number κ_s of the sampling spatial scale as $\kappa_s = 2\pi f_s / v_z$. Figure 3 shows three profiles of simulated S_4 values, where the saturated S_4 values are equal to 0.8, 0.5, and 0.2 separately, as functions of a normalized sampling wave number κ_s / κ_F . Three simulated S_4 profiles present results for different cases of strong, moderate, and weak scintillations, separately. Notably, when the wave number κ_s of the sampling spatial scale is larger than the wave number κ_F at the FFZ, saturation of the scintillation index S_4 becomes apparent because of the power-law spectrum of electron density fluctuation, in the order of $-p$. We could conclude that the S_4 values are "complete" when κ_s is larger than κ_F , i.e., the sampling spatial scale is less than the FFZ. However, for values of κ_s less than κ_F , the S_4 values decrease as the logarithm of κ_s decreases. This means that the derived S_4 values could be underestimated when the sampling spatial scale is larger than the FFZ, i.e., in "undersampling" conditions.

Another parameter used to identify the Es layer from GPS/GNSS RO observations [8–11] is the normalized signal amplitude standard deviation σ_A , which would be equivalent to the S_2 index [22]. We apply Ryton approximation to derive a wave amplitude $u_a = u_0 \exp(\chi)$. Assuming that the logarithmic amplitude χ of the wave field through an Es layer slab has a normal distribution with a mean of zero, we define S_2 as follows:

$$S_2^2 = \frac{\langle (u_a - \langle u_a \rangle)^2 \rangle}{\langle u_a \rangle^2} = \frac{\langle u_0^2 \exp(2\chi) \rangle}{\langle u_0 \exp(\chi) \rangle^2} - 1 \approx \frac{\langle \chi^2 \rangle + \frac{3}{2}\langle \chi^2 \rangle^2}{1 + \langle \chi^2 \rangle + \frac{1}{2}\langle \chi^2 \rangle^2}. \quad (14)$$

Being similar to the scintillation index S_4 , the square of the normalized signal amplitude standard deviation S_2 is a function of the log amplitude departure correlation of wave field, i.e., $\langle \chi^2 \rangle$. For weak scintillations, i.e., $\langle \chi^2 \rangle \ll 1$, $S_2^2 \sim \langle \chi^2 \rangle$, and the S_2 value is approximately half that of S_4 and equal to the square root of the integral of the log amplitude departure spectra in the spatial scale. Figure 3 shows another three profiles of simulated S_2 values, corresponding to three complete S_4 values equal to 0.8, 0.5, and 0.2 separately, as functions of the normalized sampling wave number κ_s / κ_F . Notably, being similar to S_4 , the normalized signal amplitude standard deviation S_2 values are saturated, and are complete when κ_s is larger than κ_F . However, for the values of κ_s less than κ_F , the S_2 values decrease as the logarithm of κ_s is decreasing. This also means that the derived S_2 values are underestimated when the sampling spatial scale is larger than the FFZ. Figure 3

also shows three profiles of simulated S_2/S_4 values, corresponding to three complete S_4 values equal to 0.8, 0.5, and 0.2 separately, as functions of the normalized sampling wave number κ_s/κ_F . Notably, the three profiles of simulated S_2/S_4 ratios are mostly overlapped, and all simulated S_2 values are approximately half of the simulated S_4 values for different complete S_4 values, whenever κ_s is larger or less than κ_F .

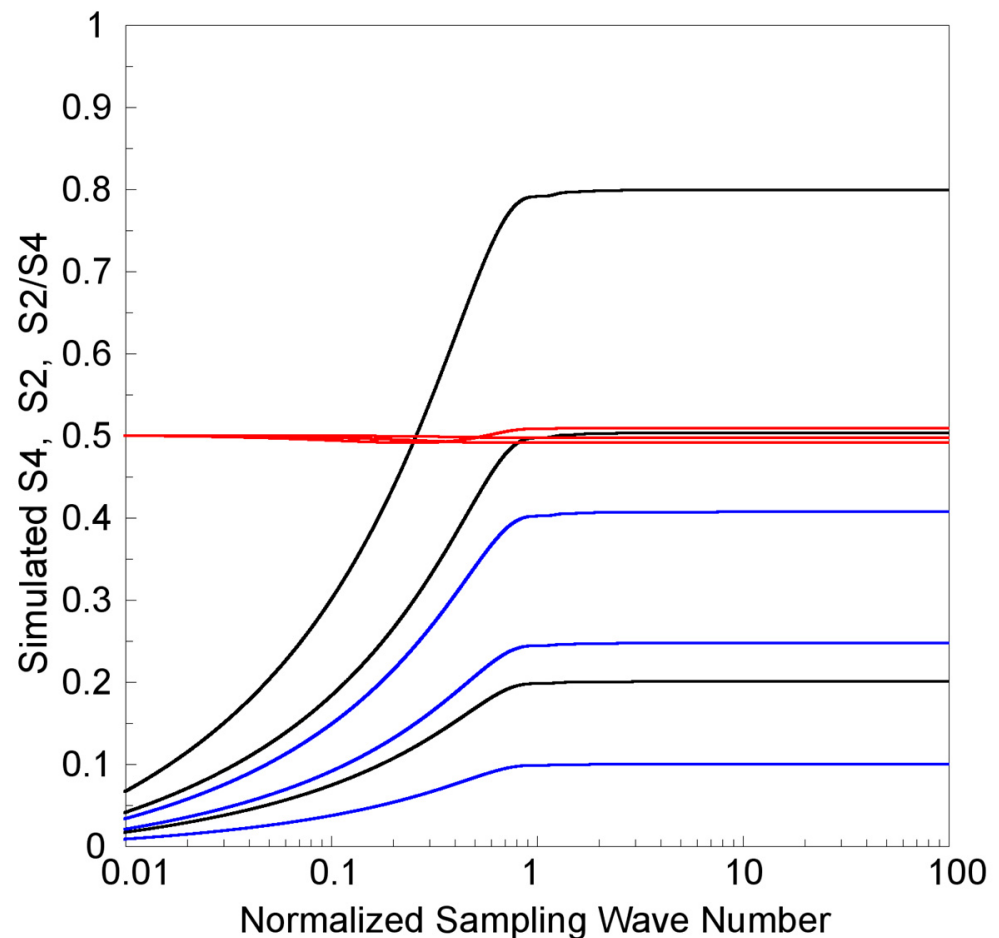


Figure 3. For different complete (saturated) S_4 values of 0.8, 0.5, and 0.2, simulated scintillation index S_4 (shown as the black lines) and normalized signal amplitude standard deviation S_2 (shown as the blue lines) as functions of a normalized sampling wave number κ_s/κ_F in the log scale are shown from top to bottom separately. The ratio of S_2/S_4 as functions of κ_s/κ_F are also shown as the red lines, but almost overlap around a value of 0.5.

3. Results

The FS3/COSMIC is a joint Taiwan–U.S. mission consisting of six identical LEO micro-satellites from mid-2006 to 2019. Each spacecraft carried a GPS receiver developed by the Jet Propulsion Laboratory (JPL) and utilized four GPS antennas: two limb viewing occultation antennas remotely sensing the atmosphere and low ionosphere at 50 Hz from the Earth surface up to approximately 125 km, and two slant observing antennas for precise orbit determination (POD) and remotely sensing the ionosphere at 1 Hz [23]. Therefore, the use of both limb viewing and POD antennas could produce simultaneous occultation observations consisting of two sets of 50 Hz and 1 Hz limb viewing links separately with different altitude resolutions of approximately 0.064 and 3.2 km at E-region altitudes. Both the GPS RO measurements include GPS and LEO satellite orbits, carrier excess phase and carrier signal–noise ratio (SNR) amplitudes for dual GPS L-band signals ($f_1 = 1575.42$ MHz and $f_2 = 1227.60$ MHz) at 50 Hz and 1 Hz, i.e., the “atmPhs” and “ionPhs” data, respectively. Notably, the FS3/COSMIC also provides 1 Hz amplitude scintillation S_4 data at the L1

band as the “scnLv1” data. The amplitude scintillation measurements are performed by an on-board algorithm under a Gaussian distribution assumption applied to the raw 50 Hz L1-band SNR amplitude data (Syndergaard 2006, COSMIC S4 data, from the website: http://cdaac-www.cosmic.ucar.edu/cdaac/doc/documents/s4_description.pdf, accessed on 22 August 2021). The on-board S_4 measurements are not derived by the scintillation index definition shown in Equation (12), and are thus not discussed in this study.

As described in the last section, the FFZ D_F of a GPS RO observation on the Es layer is approximately 0.8 km. This means that a 50 Hz limb viewing setting can be used to determine the complete scintillation index S_4 and S_2 values upon Es layer observation, but a 1 Hz limb viewing cannot. Figure 4 shows one example of FS3/COSMIC “atmPhs” (50-Hz) RO observation with an Es event recorded on 1 January 2007. As shown, significant amplitude fluctuations from L1-band signals were observed at E-region altitudes, and the corresponding S_4 and S_2 altitudinal profiles can be derived by Equations (12) and (14) separately applied to a sliding window of 4 s amplitude data. However, the L2-band signals are much weaker and have insufficient sensitivity to derive reliable S_4 and S_2 values to be shown. Notably, there is strong scintillation in the Es event, and the peak S_4 (S_2) value is 0.82 (0.39) for the GPS L1-band signals.

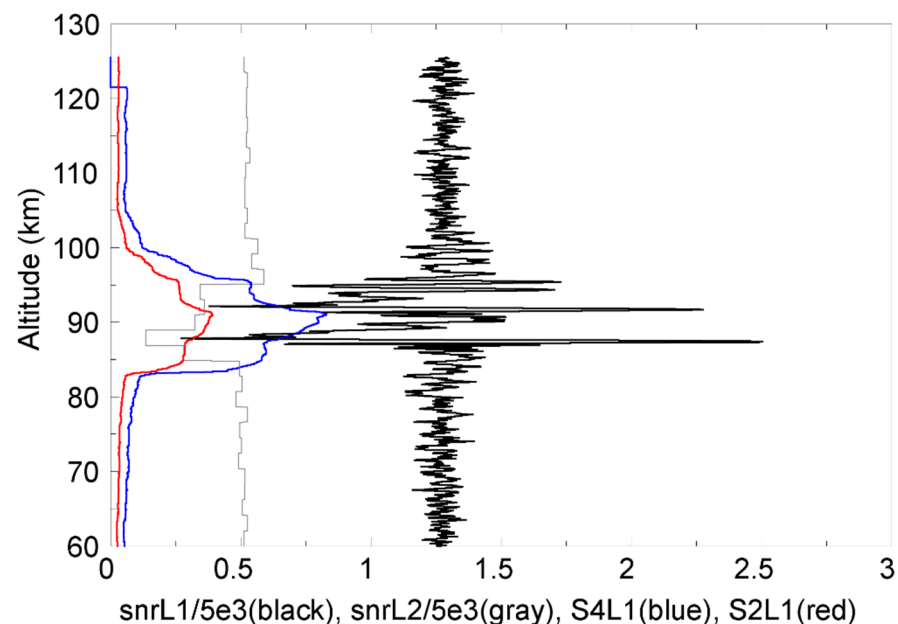


Figure 4. One example of FS3/COSMIC GPS RO observation with an Es event. The limb viewing L1- and L2-band SNR amplitudes of 50 Hz data versus GPS-LEO tangent point altitudes are shown in black and gray, respectively. The resulting S_4 and S_2 altitudinal profiles of GPS L1-band signals are also shown in blue and red, respectively. Notably, the peak S_4 (S_2) value is 0.82 (0.39).

As mentioned, 50 Hz GPS-LEO limb viewing has a vertical sampling spatial scale of approximately 0.064 km, which is over one order less than the FFZ (~ 0.8 km) of the Es layer RO observation. We can perform de-sampling to obtain more sets of amplitude data at different sampling frequencies of $50/n$ Hz, where $n = 1, 2, \dots, 100$. The resulting one hundred sets of amplitude data can be used to derive different altitudinal S_4 and S_2 profiles using a 4 s sliding window, and obtain corresponding peak S_4 and S_2 values at sampling frequencies from 0.5 to 50 Hz, which are approximately equal to normalized sampling spatial scales κ_s/κ_F of 0.2 to 20. Figure 5 shows the measured peaks S_4 , S_2 , and their ratio S_2/S_4 values as a function of κ_s/κ_F based on the FS3/COSMIC RO amplitude data, as used in Figure 4. Notably, the measured peak S_4 and S_2 profiles in κ_s/κ_F fluctuate but are mainly similar to the simulated S_4 and S_2 profiles in the strong scintillation case of a complete S_4 value of 0.8, as shown in Figure 3. The S_4 and S_2 values are saturated to ~ 0.8 and ~ 0.4 , respectively, when κ_s is larger than κ_F , and, when κ_s is less than κ_F , the S_4

and S_2 values decrease in general as the logarithm of κ_s decreases. Figure 5 also shows the measured S_2/S_4 values to be more or less than 0.5 at different normalized sampling wave numbers κ_s/κ_F from 0.2 to 20, i.e., the measured S_2 values are also approximately half of the measured S_4 values whenever κ_s is larger or less than κ_F .

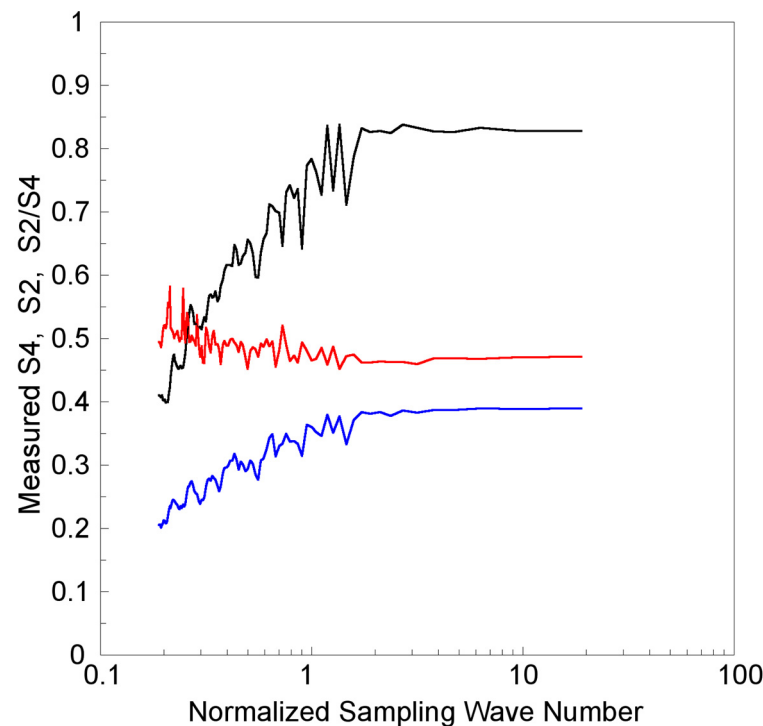


Figure 5. The dependence on normalized sampling wave number κ_s/κ_F for peak S_4 (in black), S_2 (in blue), and their ratio S_2/S_4 (in red). The experimental amplitude data are the same as those used in Figure 4.

The FS3/COSMIC program performed more than one thousand complete 50 Hz GPS RO E-region observations per day from mid-2006 to the end of 2016. There were more than two thousand complete E-region observations per day in the years from 2007 to 2009, but, after 2016, the RO observation number decreased to a few hundred per day in 2019. Ref. [11] determined that around 30% of those observations were Es events, based on the criteria of its peak S_2 value (>0.2) and altitude (>80 km and less than the top altitude of each 50 Hz GPS RO observation). The local Es event occurrence rate could approach 70% during hemispheric summer seasons. To determine the dependence on the sampling spatial scale of Es layer scintillation index determinations, the top, middle, and bottom panels of Figure 6 show the peak S_4 and S_2 , and their S_2/S_4 ratio values, as a function of the normalized sampling wave number for three cases of strong scintillations (complete $S_4 \sim 0.8(\pm 0.01)$ and 35 observations), moderate scintillations (complete $S_4 \sim 0.5(\pm 0.01)$ and 57 observations), and weak scintillations (complete $S_4 \sim 0.2(\pm 0.01)$ and 143 observations), respectively. The experimental 50 Hz FS3/COSMIC data were obtained on 1 January and 1 July 2007, and comprise 4750 GPS RO observations totally. Each RO observation was de-sampled into one hundred sets of amplitude profiles used to derived corresponding peak S_4 , S_2 , and S_2/S_4 values with different sampling frequencies from 0.5 to 50 Hz, i.e., normalized sampling wave numbers κ_s/κ_F from approximately 0.2 to 20. Generally, as shown in Figure 6, there was a greater spread of peak S_4 , S_2 , and S_2/S_4 values when sampling wave number was less. This is reasonable, because the mean error increases as its sampled number decreases, i.e., the sampling frequency decreases, and the same 4 s sampling window is used. However, the dependence on sampling spatial scale of the S_4 , S_2 , and S_2/S_4 values is similar to that of the simulated S_4 , S_2 , and S_2/S_4 profiles,

shown in Figure 3, regardless of whether the scintillation cases are strong (complete $S_4 \sim 0.8$), moderate (complete $S_4 \sim 0.5$), or weak (complete $S_4 \sim 0.2$).

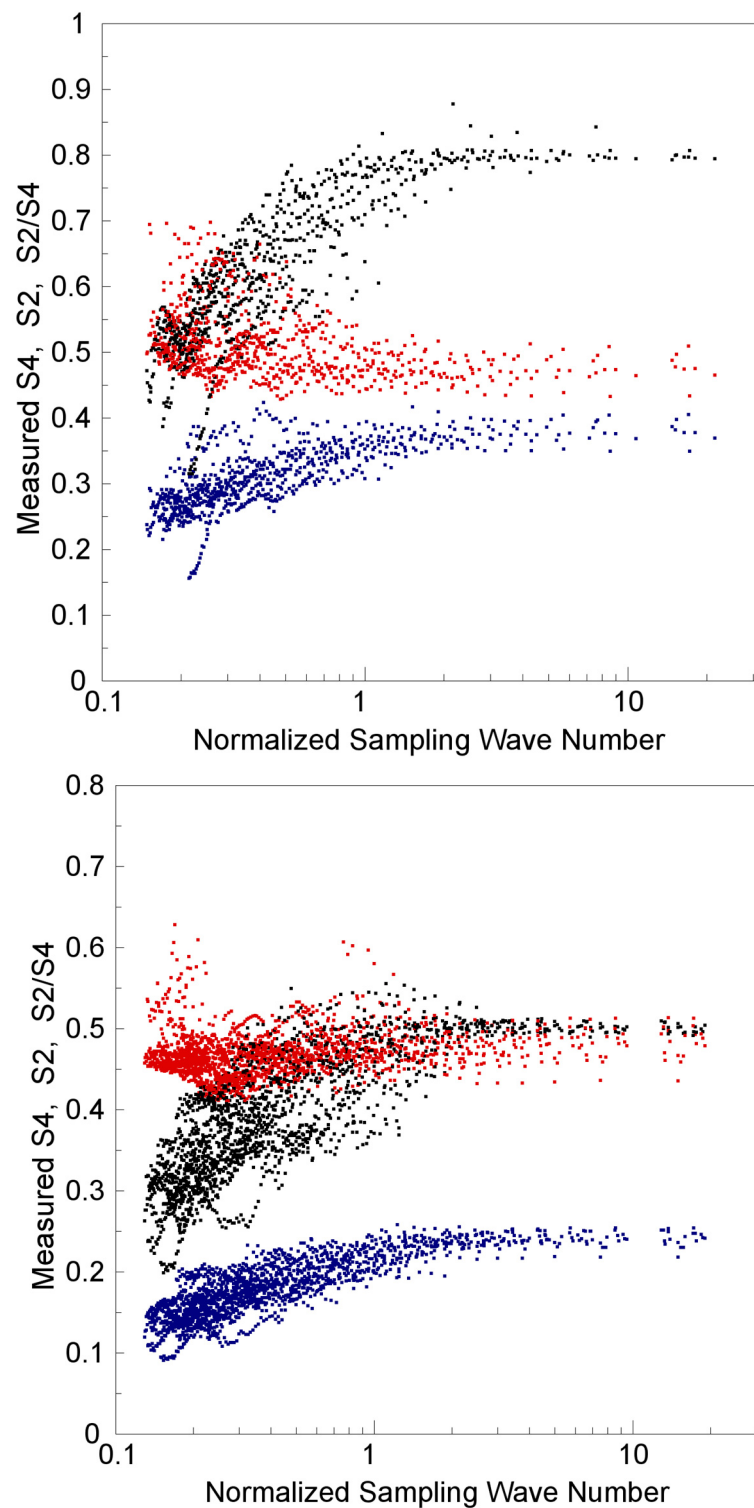


Figure 6. Cont.

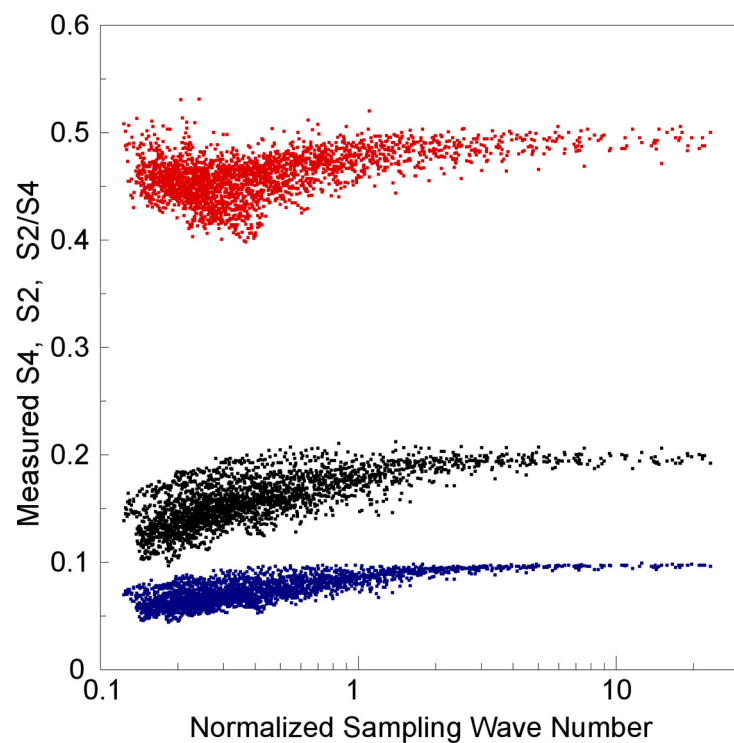


Figure 6. Measured Es layer S_4 , S_2 , and their ratio S_2/S_4 values as a function of the normalized sampling wave number for three cases of strong scintillations (complete $S_4 \sim 0.8$, top panel), moderate scintillations (complete $S_4 \sim 0.5$, middle panel), and weak scintillations (complete $S_4 \sim 0.2$, bottom panel). The experimental FS3/COSMIC data were obtained on 1 January and 1 July 2007.

4. Discussions

Following the FS3/COSMIC mission, a follow-on program called FormoSat-7 (FS7)/COSMIC2 is in progress, with satellites launched on 25 June 2019. Similar to the FS3/COSMIC, the FS7/COSMIC2 is a six-LEO-satellite constellation mission orbiting at 24° inclination and 520~720-km altitude. It enhances GNSS receiver capability to accommodate signals from GPS and GLONASS satellites, and can provide more than 5000 RO observations per day within the region between geographic latitudes of $\pm 40^\circ$. The large dataset from the FS7/COSMIC2 program enables precise specifications and statistical studies on equatorial and low-latitude ionospheric electron densities and irregularities. Notably, each LEO satellite of FS7/COSMIC2 also carries two limb viewing occultation antennas remotely sensing the atmosphere at 50 Hz, and another two slant observing antennas for POD and remotely sensing the ionosphere at 1 Hz. However, the altitude data of GPS/GNSS RO 50 Hz “atmPhs” are distributed between the Earth’s surface and a 60 km altitude, and do not include the E region range because of mission data storage constraints and satellite downlink bandwidth limitations [24]. This means that Es layer observations by FS7/COSMIC2 can be performed using 1 Hz “ionPhs” data only, and the S_4 and S_2 values derived by Equations (12) and (14) are underestimated under undersampling conditions and are not complete. Therefore, it is necessary to find a method for solving the underestimated scintillation indexes (S_4 and S_2).

To illustrate and compare the complete and undersampled scintillation observations, Figure 7 shows two scatter plots and the corresponding least-squares fitting lines for the measured peak S_4 and S_2 values using 1 Hz FS3/COSMIC data versus the peak S_4 and S_2 values measured using 50 Hz FS3/COSMIC data, respectively, on E and Es layer observations. The experimental FS3/COSMIC data were recorded on 1 January and 1 July 2007, and the 1 Hz amplitudes have been de-sampled from the 50 Hz amplitudes of “atmPhs” data. The results show that the peak S_4 (S_2) measurements of E and Es layer observations using 50 Hz and de-sampled 1 Hz amplitude data have very high correlation coefficients

of 0.95 (0.97). Meanwhile, from the least-squares fitting line equations shown in Figure 7, we see that the underestimated S_4 (S_2) values derived from the 1 Hz data have a ratio of 0.77 (0.84) to the complete S_4 (S_2) values derived from 50 Hz data. The strong correlations prove the reliability of complete S_4 and S_2 determinations using undersampled S_4 and S_2 measurements and corresponding sampling frequency or spatial scale information. Notably, the normalized spatial wave number κ_s/κ_F is approximately 0.4 at a limb-viewing sampling rate of 1 Hz on the E or Es layer RO observations. The resulting ratio of 0.77 (0.84) is close to the ratio of ~ 0.8 for the simulated S_4 (S_2) value (at a κ_s/κ_F of 0.4, as shown in Figure 3) to the complete S_4 (S_2) value, regardless of whether the scintillation cases are strong (complete $S_4 \sim 0.8$), moderate (complete $S_4 \sim 0.5$), or weak (complete $S_4 \sim 0.2$). Furthermore, as shown in Figure 7, the measured complete S_2 values are distributed from 0.07 to 0.5, approximately half of the measured complete S_4 distribution range from 0.15 to 1.0. Figure 8 shows another two scatter plots and the corresponding least-squares fitting lines for the peak S_2 values versus peak S_4 values measured using 50 Hz and de-sampled 1 Hz FS3/COSMIC “atmPhs” data separately in E and Es layer observations. The experimental data are the same as those used in Figure 7. The results show that the peak S_2 versus S_4 measurements for the E and Es layers have very high correlation coefficients of 0.98 and 0.97 using 50 Hz and de-sampled 1 Hz amplitude data, respectively. Meanwhile, from the least-squares fitting line equations shown in Figure 8, we see that the slopes of both fitting lines, i.e., the mean ratios of peak S_2 to S_4 values, are approximately equal to 0.5, which is the same as the simulated S_2/S_4 values shown in Figure 3. This means that the scintillation index S_4 and the normalized signal amplitude standard deviation S_2 measurements have high correlations with the determined ionospheric scintillation level.

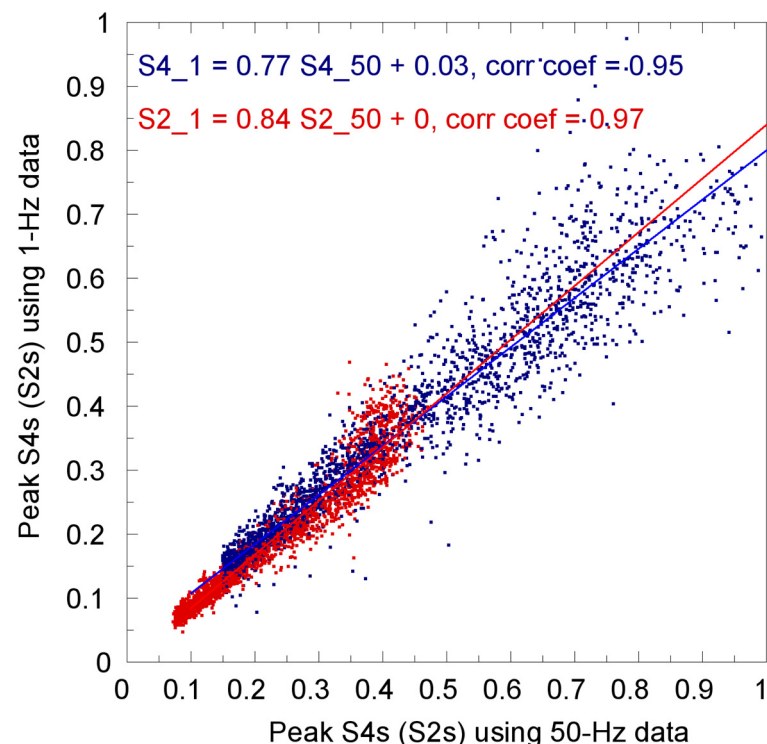


Figure 7. Scatter plot for the peak S_4 (S_2) values measured using 1 Hz data versus the peak S_4 (S_2) values measured using 50 Hz data is shown in blue (red). Two corresponding least-squares fitting lines, line equations, and the obtained correlative coefficients are also shown. The experimental FS3/COSMIC data were obtained on 1 January and 1 July 2007.

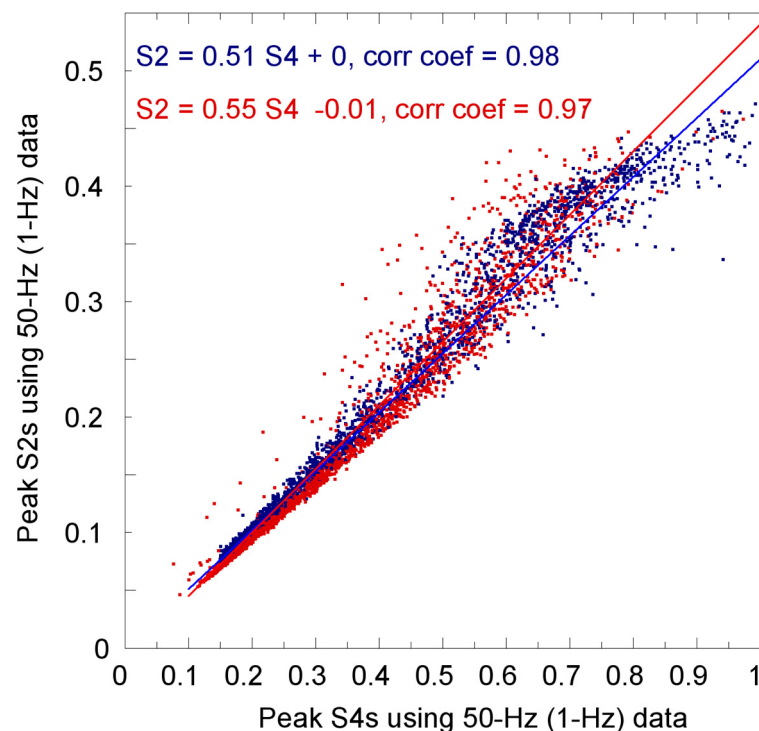


Figure 8. Scatter plot for the peak S_2 values measured using 50 Hz (1-Hz) data versus the peak S_4 values measured using 50 Hz (1-Hz) data is shown in blue (red). Two corresponding least-squares fitting lines, line equations, and the obtained correlative coefficients are also shown. As in Figure 7, the experimental FS3/COSMIC data were obtained on 1 January and 1 July 2007.

5. Conclusions

The diffraction theory of wave propagation in a stationary random medium establishes a connection between the spatial spectrum of ionospheric electron density fluctuations and the power spectrum of observed signal intensities, and therefore the amplitude scintillations. We have reported in this paper on the relevant theories and FS3/COSMIC experiments of radio wave scintillations of Es layer RO observations. The theoretical results show that applying Ryton approximation to radio wave propagations through an Es layer irregularity slab can provide reasonable descriptions of weak-, moderate-, and strong-amplitude scintillations. We conclude that a GPS RO scintillation observation is complete when the sampling spatial scale is less than the FFZ, otherwise it is a case of undersampling. It is shown that the simulated results are consistent with interpretations of FS3/COSMIC RO scintillation index estimates in terms of the different sampling frequencies. It is useful to clarify the dependence of the determination of the scintillation index on the sampling spatial scale, and find a method for solving complete scintillation indices (S_4 and S_2) under undersampling conditions.

Author Contributions: Conceptualization, L.-C.T., S.-Y.S., C.-H.L., H.S. and J.W.; methodology, L.-C.T., S.-Y.S. and C.-H.L.; software, L.-C.T.; validation, L.-C.T., S.-Y.S., C.-H.L., H.S. and J.W.; formal analysis, L.-C.T.; investigation, L.-C.T., S.-Y.S., H.S. and J.W.; resources, L.-C.T., S.-Y.S., H.S. and J.W.; data curation, L.-C.T., J.W. and M.M.A.; writing—original draft preparation, L.-C.T.; writing—review and editing, L.-C.T., S.-Y.S., C.-H.L., H.S., J.W. and M.M.A.; supervision, S.-Y.S., C.-H.L., H.S. and J.W.; project administration, L.-C.T., S.-Y.S., H.S. and M.M.A.; funding acquisition, L.-C.T., S.-Y.S., H.S. and M.M.A. All authors have read and agreed to the published version of the manuscript.

Funding: This research was funded by the Ministry of Science and Technology, Taiwan (grant number MOST 107-2111-M-008-030), the Asian Office of Aerospace Research and Development of the U.S. Air Force Office of Scientific Research (grant number AOARD/ARFL FA2386-18-1-0115), and the German Research Foundation (grant number SCHU 1103/15-1).

Institutional Review Board Statement: Not applicable.

Informed Consent Statement: Not applicable.

Data Availability Statement: The FS3/COSMIC “atmPhs” data can be downloaded from the COSMIC Data Analysis and Archive Center (CDAAC, <http://cdaac-www.cosmic.ucar.edu/>, accessed on 22 August 2021) and the Taiwan Analysis Center for COSMIC (TACC, <http://tacc.cwb.gov.tw/cdaac/>, accessed on 22 August 2021).

Acknowledgments: The work was possible thanks to a free access to FS3/COSMIC archives.

Conflicts of Interest: The authors declare no conflict of interest.

References

1. Whitehead, J.D. Recent work on mid-latitude and equatorial sporadic E. *J. Atmos. Terr. Phys.* **1989**, *51*, 401–424. [[CrossRef](#)]
2. Whitehead, J.D. Report on the production and prediction of Sporadic E. *Rev. Geophys. Space Phys.* **1970**, *8*, 65. [[CrossRef](#)]
3. Yeh, K.C.; Liu, C.H. Radio wave scintillations in the ionosphere. *Proc. IEEE* **1982**, *70*, 324–360. [[CrossRef](#)]
4. Mathews, J.D. Sporadic E: Current views and recent progress. *J. Atmos. Solar-Terr. Phys.* **1998**, *60*, 413–435. [[CrossRef](#)]
5. Zeng, Z.; Sokolovskiy, S. Effect of sporadic E clouds on GPS radio occultation signals. *Geophys. Res. Lett.* **2010**, *37*, L18817. [[CrossRef](#)]
6. Ogawa, T.; Suzuki, A.; Kunitake, M. Spatial distribution of mid-latitude sporadic E scintillation in summer daytime. *Radio Sci.* **1989**, *24*, 527–538. [[CrossRef](#)]
7. Hocke, K.; Igarashi, K.; Nakamura, M.; Wilkinson, P.; Wu, J.; Pavelyev, A.; Wickert, J. Global sounding of sporadic E layers by the GPS/MET radio occultation experiment. *J. Atmos. Solar-Terr. Phys.* **2001**, *63*, 1973–1980. [[CrossRef](#)]
8. Wu, D.L.; Ao, C.O.; Hajj, G.A.; Juarez, M.D.L.T.; Mannucci, A.J. Sporadic E morphology from GPS-CHAMP radio occultation. *J. Geophys. Res.* **2005**, *110*, A01306. [[CrossRef](#)]
9. Arras, C.; Wickert, J.; Beyerle, G.; Heise, S.; Schmidt, T.; Jacobi, C. A global climatology of ionospheric irregularities derived from GPS radio occultation. *Geophys. Res. Lett.* **2008**, *35*, L14809. [[CrossRef](#)]
10. Arras, C.; Wickert, J. Estimation of ionospheric sporadic E intensities from GPS radio occultation measurements. *J. Atmos. Solar-Terr. Phys.* **2018**, *171*, 60–63. [[CrossRef](#)]
11. Tsai, L.-C.; Su, S.-Y.; Liu, C.-H.; Schuh, H.; Wickert, J.; Alizadeh, M.M. Global morphology of ionospheric sporadic E layer from the FormoSat-3/COSMIC GPS radio occultation experiment. *GPS Solut.* **2018**, *22*, 118. [[CrossRef](#)]
12. Tatarskiĭ, V.I. *The Effects of the Turbulent Atmosphere on Wave Propagation*; National Technical Information Service: Springfield, VA, USA, 1971.
13. Crane, R.K. Spectra of ionospheric scintillation. *J. Geophys. Res.* **1976**, *81*, 2041–2050. [[CrossRef](#)]
14. Rino, C.L. A power law phase screen model for ionospheric scintillation, 1. Weak scatter. *Radio Sci.* **1979**, *14*, 1135–1145. [[CrossRef](#)]
15. Rino, C.L. A power law phase screen model for ionospheric scintillation, 2. Strong scatter. *Radio Sci.* **1979**, *14*, 1147–1155. [[CrossRef](#)]
16. Priyadarshi, S. A review of ionospheric scintillation models. *Surv. Geophys.* **2015**, *36*, 295–324. [[CrossRef](#)]
17. Shkarofsky, I.P. Generalized turbulence space-correlation and wave-number spectrum—Function pairs. *Can. J. Phys.* **1968**, *46*, 2133–2153. [[CrossRef](#)]
18. Booker, H.G.; Ratcliffe, J.A.; Shinn, D.H. Diffraction from an irregular screen with applications to ionospheric problems. *Philos. Trans. Roy. Soc. London Ser. A* **1950**, *242*, 579–607.
19. Brown, W.P. Validity of the Ryton approximation. *J. Opt. Soc. Amer.* **1967**, *57*, 1539–1543. [[CrossRef](#)]
20. Fried, D.L. Test of the Ryton approximation. *J. Opt. Soc. Amer.* **1967**, *57*, 268–269. [[CrossRef](#)]
21. Wernik, A.W.; Liu, C.H. Application of the scintillation theory to ionospheric irregularities studies. *Artif. Satell.* **1975**, *10*, 37–58.
22. Strangeways, H.J. Determining scintillation effects on GPS receivers. *Radio Sci.* **2009**, *44*, RS0A36. [[CrossRef](#)]
23. Schreiner, W.; Rocken, C.; Sokolovskiy, S.; Syndergaard, S.; Hunt, D. Estimates of the precision of GPS radio occultation from the COSMIC/FORMOSAT-3 mission. *Geophys. Res. Lett.* **2007**, *34*, L04808. [[CrossRef](#)]
24. Schreiner, W.S.; Weiss, J.P.; Anthes, R.A.; Braun, J.; Chu, V.; Fong, J.; Hunt, D.; Kuo, Y.-H.; Meehan, T.; Serafino, W.; et al. COSMIC-2 radio occultation constellation: First results. *Geophys. Res. Lett.* **2020**, *47*, e2019GL086841. [[CrossRef](#)]